

Influence of the Degree of Crystallinity on the Dispersion of the Optical Parameters of $\text{Ge}_2\text{Sb}_2\text{Te}_5$ Phase-Change Memory Thin Films

M. E. Fedyanina^{a,*}, P. I. Lazarenko^a, Yu. V. Vorobyov^b, S. A. Kozyukhin^c, A. A. Dedkova^a,
A. O. Yakubov^a, V. S. Levitskii^d, I. V. Sagunova^a, and A. A. Sherchenkov^a

^a National Research University of Electronic Technology MIET, Moscow, 124498 Russia

^b Ryazan State Radio Engineering University, Ryazan, 390005 Russia

^c Kurnakov Institute of General and Inorganic Chemistry, Russian Academy of Sciences, Moscow, 119907 Russia

^d R and D Center of Thin-Film Technologies in Energetics, Ltd., St. Petersburg, 194021 Russia

*e-mail: fedyanina.m@org.miet.ru

Received February 14, 2020; revised February 14, 2020; accepted March 17, 2020

Abstract—Extensive studies of $\text{Ge}_2\text{Sb}_2\text{Te}_5$ material are associated with the possibility of producing multilevel nonvolatile elements for high-speed integrated optical functional circuits. The principle of multilevel recording in such devices is based on the formation of partially crystallized regions with substantially different optical properties in $\text{Ge}_2\text{Sb}_2\text{Te}_5$ thin films. To predict the parameters of the effect initiating phase transformations and to reliably provide a reversible transition between many logic states, it is necessary to have reliable data on the optical characteristics of $\text{Ge}_2\text{Sb}_2\text{Te}_5$ thin films in states with different degrees of crystallinity and on the conditions of attainment of such states. In the study, the influence of the phase state of $\text{Ge}_2\text{Sb}_2\text{Te}_5$ films on the extinction coefficient and refractive index and variations in the optical band gap in relation to the temperature of heat treatment are investigated. $\text{Ge}_2\text{Sb}_2\text{Te}_5$ thin-film samples are examined by means of atomic-force microscopy, X-ray phase analysis, and energy-dispersive microanalysis to determine the film thickness, morphology, phase state, and composition. By spectroscopic ellipsometry, the spectra of the ellipsometric angles ψ and Δ (the amplitude and phase components of the light wave) are obtained, and the extinction coefficient and refractive index are determined. The influence of the layer models and mathematical models on calculation of the dispersions of the optical parameters of $\text{Ge}_2\text{Sb}_2\text{Te}_5$ films is considered. A substantial increase in the extinction coefficient and refractive index at the wavelength 1550 nm on heat treatment at temperatures higher than 200°C is established. It is shown that the optical band gaps of $\text{Ge}_2\text{Sb}_2\text{Te}_5$ thin films in the amorphous and crystalline states are 0.71 and 0.47 eV, respectively. It is found that the dependences of the extinction coefficient, refractive index, and band gap on the degree of crystallinity of $\text{Ge}_2\text{Sb}_2\text{Te}_5$ thin films are close to linear.

Keywords: multilevel devices, nanophotonics, phase-change memory, thin films, $\text{Ge}_2\text{Sb}_2\text{Te}_5$, ellipsometry, refractive index, extinction coefficient, optical band gap, crystallization, degree of crystallinity

DOI: 10.1134/S1063782620130060

INTRODUCTION

Over the last five years, nonvolatile electric phase-change memory (PCM) devices based on chalcogenide semiconductor compounds of the Ge–Sb–Te system have been successfully used as storage-class memory (SCM) units [1]. Electric PCM devices produced by the Intel corporation on the basis of materials of the Ge–Sb–Te system by the 3D-Xpoint, Intel Optane, technology possess a 1000-times higher operating speed compared to that of NAND flash memory [2] and a 4.5-times higher information-recording density compared to that of dynamic random access memory (DRAM) manufactured by the 20-nm technology.

As the amorphous state transforms into the crystal state upon exposure to laser-radiation pulses [3] or under the action of current [4], a substantial change in the optical properties of Ge–Sb–Te thin films is observed. The possibility of forming intermediate, partially crystallized states [5] opens up wide prospects for creating multilevel-cell (MLC) nonvolatile elements of high-speed integrated optical functional circuits that allow the recording of more than two logic states [6]. The engineering of nonvolatile nanophotonic elements capable of providing a multilevel change in the parameters of optical signals is of particular importance for the further development of nano-

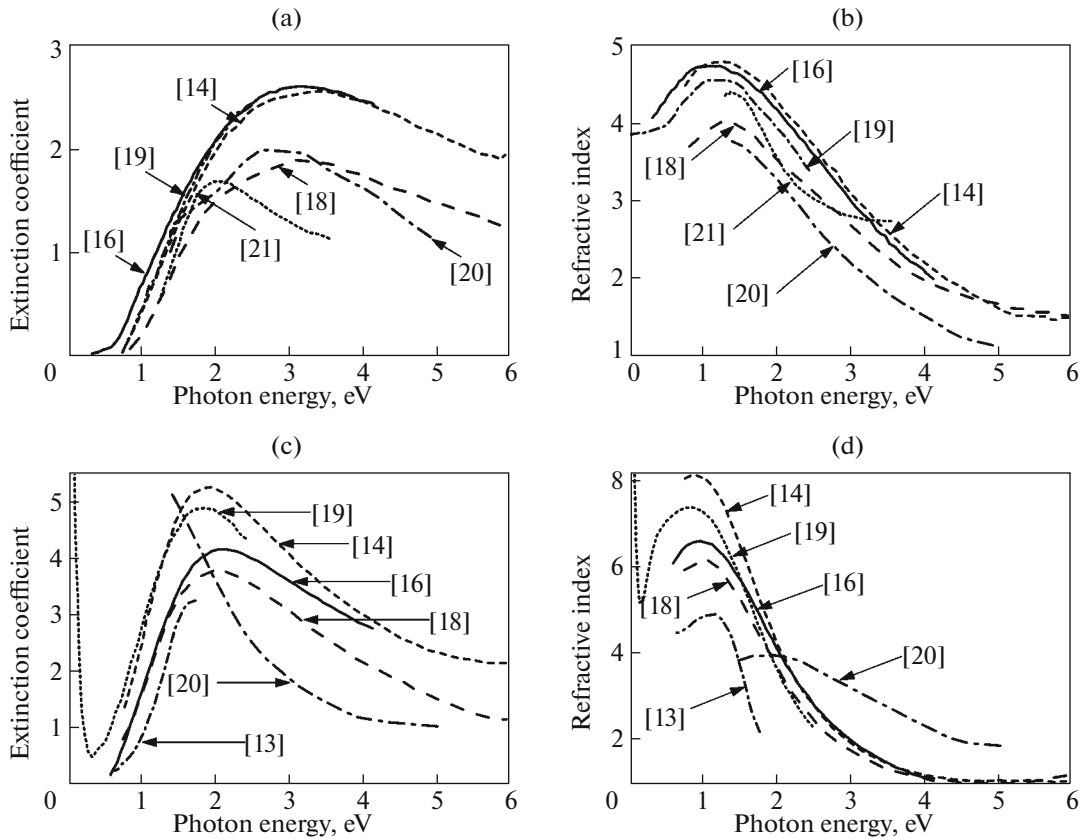


Fig. 1. Spectra of the extinction coefficient and refractive index for (a, b) the amorphous and (c, d) crystalline $\text{Ge}_2\text{Sb}_2\text{Te}_5$ thin films [13, 14, 16, 18–21].

photonics and integrated optics as well as for the creation of more efficient computing neural networks [7].

The principle of operation of reconfigurable multi-level nanophotonic PCM devices is based on the processes of crystallization and amorphization and, correspondingly, the different relationships between two phases for functional regions of thin-film materials of the Ge–Sb–Te system. These processes can be initiated by exposure to a high temperature [8], by laser radiation [3], or by an electric current [4]. By varying the parameters of the initiating effect, it is possible to form totally amorphous or totally crystalline (face-centered cubic (FCC) and hexagonal close-packed (HCP)) states as well as states with different volumes of amorphized and crystallized materials (partial crystallization) in the functional region. It is the possibility of forming states with different degrees of crystallinity and the considerable contrast between the optical properties of these states that allow the creation of a multilevel system with a reasonable signal-to-noise ratio. To date, it has been demonstrated that, in principle, it is possible to create an efficient 5-bit nonvolatile full-optical-memory element that can store more than 34 nonvolatile states in one cell [9].

When producing multilevel memory elements, one encounters a number of unsolved problems. Most studies are concerned with the optical properties of totally amorphous or totally crystalline $\text{Ge}_2\text{Sb}_2\text{Te}_5$ films; these properties define the maximum attainable optical contrast [10, 11]. Analysis of the results obtained for amorphous and crystalline samples by spectrophotometry [12] and ellipsometry (Fig. 1) shows a considerable spread of the data. Such a spread can be caused by the specific features of the production of $\text{Ge}_2\text{Sb}_2\text{Te}_5$ films, different conditions of crystallization, and different approaches and models used in the stage of processing of the experimental results; for example, the Tauc–Lorentz [13, 14], Cauchy [15], and Cody–Lorentz [16] models of the dispersion of optical constants are used.

To predict the parameters of the effect initiating phase transformations and to reliably provide a reversible transition between many logic states, it is necessary to have verifiable and reliable data on the optical parameters of $\text{Ge}_2\text{Sb}_2\text{Te}_5$ films in states with different degrees of crystallinity and on the conditions of production of such films. At the same time, measurements should be performed under identical conditions, which allows one to exclude additional errors

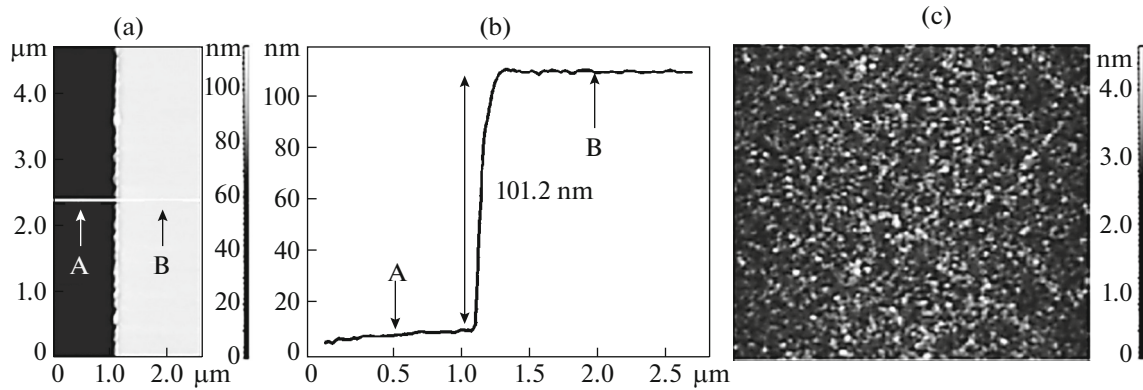


Fig. 2. AFM results: (a) image of the stepwise surface, (b) the cross-section profile of the step (with indication of the film thickness), and (c) the surface morphology of the as-deposited $\text{Ge}_2\text{Sb}_2\text{Te}_5$ thin film.

associated, for example, with the thermal-optical effect [17].

The results of studying the optical properties of partially crystallized $\text{Ge}_2\text{Sb}_2\text{Te}_5$ films by spectrophotometry are reported in [12]. The ellipsometry technique allows one to determine the ellipsometric angles ψ and Δ that describe the elliptical polarization of light reflected from the interfaces of a multilayer sample. Then, with the use of an appropriate model, one can quickly determine the optical parameters (refractive index and extinction coefficient) of thin films formed on nontransparent substrates. This procedure is distinguished by a high sensitivity to surface features. Compared to the spectrophotometric methods, this technique provides a higher accuracy, since there is no need to measure the transmittance and reflectance of highly absorbing $\text{Ge}_2\text{Sb}_2\text{Te}_5$ thin films.

The purpose of this study is to investigate the optical properties of amorphous, partially crystallized, and crystalline $\text{Ge}_2\text{Sb}_2\text{Te}_5$ thin films by means of ellipsometry.

EXPERIMENTAL

We studied $\text{Ge}_2\text{Sb}_2\text{Te}_5$ thin films formed by the magnetron sputtering of a polycrystalline target. During deposition, the argon pressure was 5.7×10^{-1} Pa, and the power was 100 W. For substrates, we used *n*-Si:B wafers with a resistivity of $\rho = 12 \Omega \text{ cm}$.

The testing of as-deposited $\text{Ge}_2\text{Sb}_2\text{Te}_5$ thin-film samples with a Solver P47-Pro atomic-force microscope (AFM) shows that the thickness of all of the films under study is ~ 101 nm and the root-mean-square (rms) roughness is no larger than 1 nm (Fig. 2). From the results of studies with an FEI Titan Themis 200-80 transmission electron microscope (TEM) with an attachment for energy-dispersive microanalysis, it is established that the deposited films feature a uniform distribution of composition throughout the

thickness and a distribution close to that in $\text{Ge}_2\text{Sb}_2\text{Te}_5$ films. The structure of the $\text{Ge}_2\text{Sb}_2\text{Te}_5$ films was studied by X-ray phase analysis (Rigaku SmartLab). The X-ray diffraction patterns of the as-deposited amorphous $\text{Ge}_2\text{Sb}_2\text{Te}_5$ films show a characteristic amorphous halo, which suggests a noncrystalline phase of the films. At the same time, heat treatment of the thin films at a temperature of 250°C brings about the appearance of reflections, whose position is characteristic of cubically structured NaCl-type $\text{Ge}_2\text{Sb}_2\text{Te}_5$ films.

In order to determine the temperature region of crystallization and to choose the heat-treatment temperature facilitating the formation of partially crystallized samples, we studied the temperature dependences of the resistivity of $\text{Ge}_2\text{Sb}_2\text{Te}_5$ thin films in an argon flow, using a hardware–software complex system based on a Linkam HFS600E-PB4 heating table. The current was measured at a field strength of 0.77 V/cm with a rate of 1 point/s in the temperature range from room temperature to 300°C ; the heating rate was 5°C/min . From Fig. 3, it can be seen that the phase transition from the amorphous state to the crystalline state is accompanied by a decrease in the resistivity of the $\text{Ge}_2\text{Sb}_2\text{Te}_5$ thin film and occurs in the temperature range $170\text{--}200^\circ\text{C}$. With regard to these data, we selected 11 values of the heat-treatment temperature for further investigation of the samples (see Fig. 3). Heat treatment consisted in heating of the samples to one of the chosen temperatures, with subsequent cooling in an argon flow with the rate 5°C/min . No holding of the samples at the maximum temperature reached upon heating was performed.

The spectra of the ellipsometric parameters I_c and I_s which determine the characteristics of a light wave after being reflected from the sample were recorded with a Horiba Uvisel 2 spectroscopic ellipsometer in the wavelength range $200\text{--}2100 \text{ nm}$ with a wavelength step of 5 nm ; the tilt angles of the polarizer and ana-

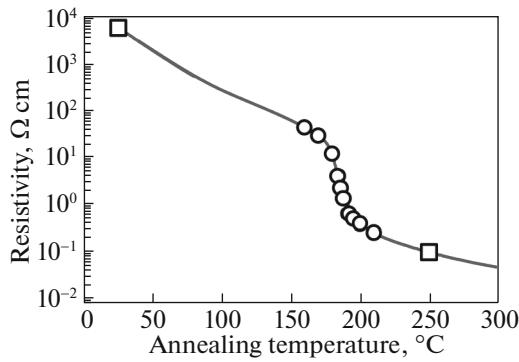


Fig. 3. Dependence of the resistivity of the Ge₂Sb₂Te₅ thin film on the annealing temperature. (Open squares and circles correspond to the annealing temperatures chosen for studies of the optical properties.)

lyzer were 70°. Using the parameters I_c and I_s , we determined the spectra of the ellipsometric angles ψ and Δ , the refractive indices n , the extinction coefficients k , the optical band gaps E_g^{opt} , and the film thicknesses. Controlling the operation of the ellipsometer during measurements and subsequent determination of the results by simulation were conducted with the use of DeltaPsi2 (Horiba) software.

RESULTS AND DISCUSSION

The spectra of the ellipsometric angles ψ and Δ were obtained for samples in the amorphous state and after heat treatment at the temperatures chosen. As an example, Figure 4 shows the results of measurements for the as-deposited amorphous sample and the sample subjected to heat treatment at a temperature of 250°C.

Using the spectral characteristics obtained with the ellipsometer and an appropriate model of the dispersion of optical constants, we can obtain the spectra of the complex refractive index and extinction coefficient,

calculate the complex dielectric function, and estimate the layer thicknesses for the samples. The choice of models of the optical constants is diverse and depends on the type of the material, the spectral region, etc. To interpret the results of the ellipsometry measurements for amorphous thin films, including Ge₂Sb₂Te₅ films, the Tauc–Lorentz [13, 14] and Cody–Lorentz [16] models are used most often.

The Tauc–Lorentz model was developed by Jellison and Modin on the basis of the Tauc density of states and the Lorentz oscillator [22]. If the photon energy E exceeds the optical band gap, the imaginary part of the dielectric function, $\epsilon_2(E)$, can be determined in this model from the relation

$$\epsilon_2(E) = T(E)L(E) = \frac{AE_0C(E - E_g^{opt})^2}{(E^2 - E_0^2)^2 + C^2E^2} \frac{1}{E},$$

$$E > E_g^{opt}.$$

If $E < E_g^{opt}$, $\epsilon_2(E) = 0$.

The Cody–Lorentz model was proposed by Ferlauto et al. [23]. The specific feature of application of this model to the calculation is inclusion of the Urbach energy that describes the extent of the density of localized states of band tails in the mobility gap of an amorphous semiconductor. The functional form of the model is defined by a system of two equations

$$\epsilon_2(E) = \frac{E_t G(E_t) L(E_t)}{E} \exp\left(\frac{E - E_t}{E_\mu}\right), \quad 0 < E \leq E_t,$$

$$\epsilon_2(E) = G(E)L(E) = \left[\frac{(E - E_g^{opt})^2}{(E - E_g^{opt})^2 + E_p^2} \right] \times \left[\frac{AE_0\Gamma E}{(E^2 - E_0^2)^2 + \Gamma^2 E^2} \right], \quad E > E_t.$$

Using the Cody–Lorentz model, one can obtain seven parameters, including the energy E_t that separates the prevailing contribution of the absorption at

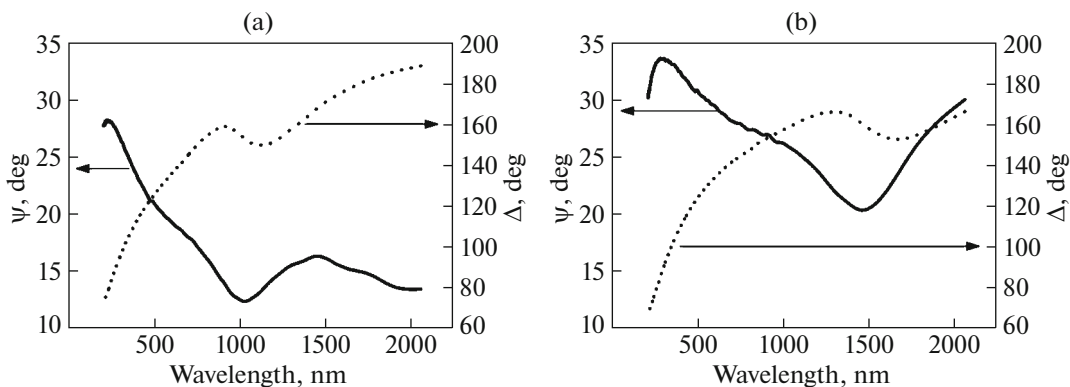


Fig. 4. Spectra of the ellipsometric angles ψ and Δ for (a) the amorphous and (b) crystalline samples.

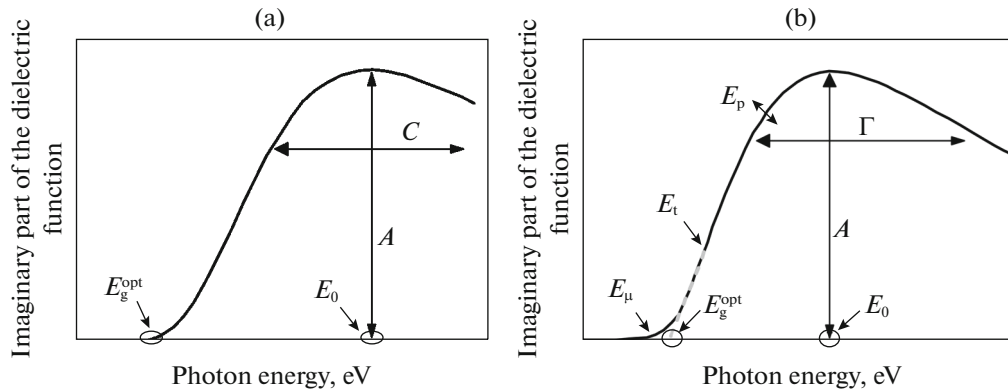


Fig. 5. Schematic illustration of the principle of determining the parameters of (a) the Tauc-Lorentz and (b) Cody-Lorentz models.

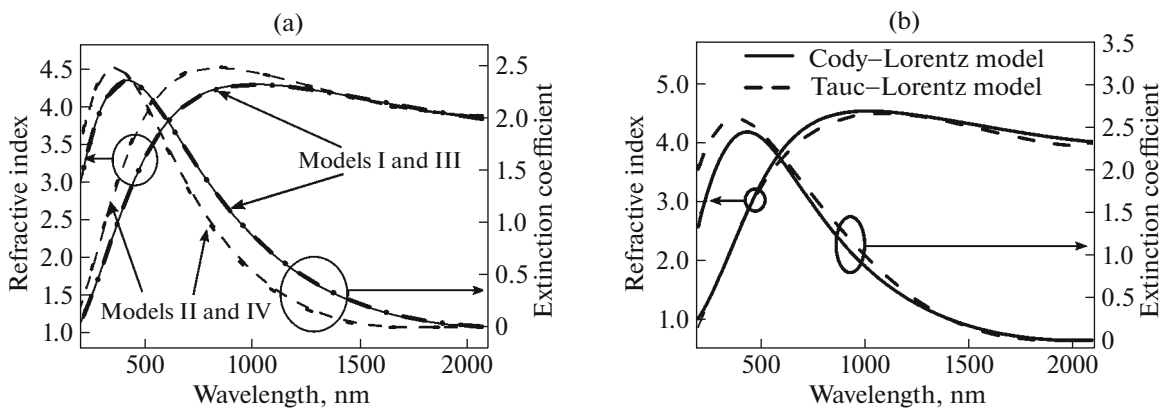


Fig. 6. Wavelength dependences of the refractive index and extinction coefficient in different (a) layer and (b) mathematical models.

localized states of the Urbach tail at $0 < E < E_t$ from the contribution of fundamental absorption at interband transitions, the energy E_p that describes the transition from absorption at $E < (E_p + E_g^{opt})$ to absorption at $E > (E_p + E_g^{opt})$ described by the Lorentz model, and the Urbach energy E_μ .

Figure 5 shows the dependences of the imaginary part of the dielectric function on the photon energy and explains the principle of determination of the following parameters: the optical band gap E_g^{opt} , the maximum of the absorption intensity A , the energy corresponding to the peak of the density of states E_0 , and the peak broadening factor C [24].

Apart from the mathematical model, the layer model of the sample substantially influences the results. The simplest case is the use of two-layer model I. In this model, the sample consists of a Si* substrate and the $Ge_2Sb_2Te_5$ thin film to be studied. However, in model I, the adjacent layers, e.g., oxides formed in air are disregarded, and it is assumed that

the film surface is ideally smooth. For this reason, we compare several layer models to judge the effect of individual layers on the result of simulation. In model II, account is taken of a surface layer that simulates the roughness of the $Ge_2Sb_2Te_5$ thin film. This layer is specified as a mixture of air and $Ge_2Sb_2Te_5$ material in the ratio 1:1. In model III, it is assumed that the surface of the $Ge_2Sb_2Te_5$ film is ideally smooth, but account is taken of the natural silicon-oxide layer sandwiched between the $Ge_2Sb_2Te_5$ film and the Si* substrate. Model IV takes into account all of the above-listed layers and can be represented by the Si*/SiO_x/Ge₂Sb₂Te₅/(Ge₂Sb₂Te₅ + air (1:1)) structure.

Using the above-described layer models and the Tauc-Lorentz model, we obtained the dependences shown in Fig. 6a and the simulation output parameters listed in Table 1.

The results of simulation are substantially influenced by the layer model, especially by consideration for the surface layer of the $Ge_2Sb_2Te_5$ film with air (1:1). The calculated dispersions of the optical parameters

Table 1. Comparison of the output parameters obtained by simulation using different layer models

Model	E_g^{opt} , eV	A	C	E_0 , eV	h_1 , nm	h_2 , nm	h_3 , nm	n_{1550}	k_{1550}
I	0.58	97.4	3.80	2.46	–	104.1	–	4.075	0.181
II	0.73	127.0	4.10	2.74	–	104.0	4.6	4.053	0.018
III	0.57	96.5	3.82	2.47	2.6	105.6	–	4.078	0.188
IV	0.71	120.6	2.64	3.95	3.0	106.5	3.5	4.049	0.031

h_1 , h_2 and h_3 are the thicknesses of the SiO_x , $\text{Ge}_2\text{Sb}_2\text{Te}_5$, and $\text{Ge}_2\text{Sb}_2\text{Te}_5 + \text{air}$ (1:1) layers, respectively, and k_{1550} and n_{1550} are the extinction coefficient and refractive index obtained at the emission wavelength 1550 nm.

Table 2. Simulated output parameters obtained for the amorphous sample

Model	E_g^{opt} , eV	A	C/Γ	E_0 , eV	E_μ , meV	h_1 , nm	h_2 , nm	h_3 , nm	n_{1550}	k_{1550}
Tauc–Lorentz	0.71	120.6	2.64	3.95	–	3.0	106.5	3.5	4.049	0.031
Cody–Lorentz	0.77	108.8	6.73	3.37	142.5	2.0	103.2	6.0	4.03	0.03

can be conventionally divided into two groups, of which one (models I and III) takes into consideration the layer simulating the roughness and the other (models II and IV) disregards this layer. A difference is obtained between the dispersions of the optical parameters and between the output parameters of simulation. For example, the optical band gaps of $\text{Ge}_2\text{Sb}_2\text{Te}_5$ films can differ by more than 15% (see Table 1). To perform further calculations, we chose model IV which gives results closest to those obtained by other methods, e.g., by spectrophotometry [12].

It should be noted that we observe a difference between the thickness obtained for the $\text{Ge}_2\text{Sb}_2\text{Te}_5$ layer with air (1:1) from the ellipsometry data by simulation in the context of model IV and the film roughness measured by atomic-force microscopy (<1 nm).

Table 3. Simulated output parameters obtained for the samples after annealing at different temperatures

T , °C	α	E_g^{opt} , eV	A	E_0 , eV	C	h_1 , nm	h_2 , nm	h_3 , nm
–	–	0.71	120.6	2.64	3.95	3.0	106.5	3.5
160	–	0.69	124.3	2.60	3.93	1.0	106.0	3.5
170	0	0.69	120.0	2.61	3.85	3.0	104.7	3.5
180	0.24	0.66	200.0	1.70	2.56	4.0	103.0	3.5
184	0.33	0.59	190.0	1.68	2.55	3.0	102.0	3.5
186	0.42	0.57	195.4	1.63	2.46	3.0	102.0	3.5
188	0.49	0.55	190.0	1.64	2.49	3.0	101.0	3.7
192	0.61	0.53	186.0	1.65	2.47	4.0	101.0	4.0
195	0.68	0.53	191.3	1.66	2.47	4.0	100.5	4.3
200	0.76	0.50	186.5	1.68	2.48	2.0	101.0	4.4
210	0.83	0.50	187.7	1.62	2.38	3.0	99.0	4.5
250	1.00	0.47	193.0	1.59	2.29	3.0	98.0	4.5

This difference arises from the use of physically different measurement methods as well as from the additional contribution of a natural oxide layer formed at the surface of the $\text{Ge}_2\text{Sb}_2\text{Te}_5$ film to the results of simulation. According to the results of secondary-ion mass spectrometry [25] and low-energy ion scattering spectroscopy [26], the thickness of this layer is ~ 5 nm.

Figure 6b shows the results obtained for the as-deposited amorphous $\text{Ge}_2\text{Sb}_2\text{Te}_5$ thin films in the context of the Tauc–Lorentz and Cody–Lorentz models. For the refractive index, the results obtained in these two models are practically the same; there are small discrepancies near the peak and at long wavelengths. However, for the extinction coefficient, there is a more substantial discrepancy at wavelengths shorter than 500 nm. The Tauc–Lorentz model gives a more linear variation in the extinction coefficient in the range 600–1300 nm. Table 2 lists the output parameters of the simulation with the use of the Tauc–Lorentz and Cody–Lorentz models for the amorphous sample.

Despite the similarity of the spectra of the refractive index and extinction coefficient, there are substantial differences between the output parameters. Such a discrepancy between the parameters was also observed in [23]. However, the optical band gaps obtained in the Tauc–Lorentz model closer correlate with the previously reported data and the results obtained for the amorphous sample by spectrophotometry [12]. For this reason, in further studies, we use the Tauc–Lorentz model.

Figure 7 shows the spectra of the refractive index and extinction coefficient for samples subjected to heat treatments at different temperatures (see Fig. 2). Table 3 lists the output parameters of simulation for the amorphous $\text{Ge}_2\text{Sb}_2\text{Te}_5$ thin-film sample and the samples subjected to heat treatment at different temperatures.

Analysis of the data shows that heat treatment at a temperature higher than 180°C induces a substantial

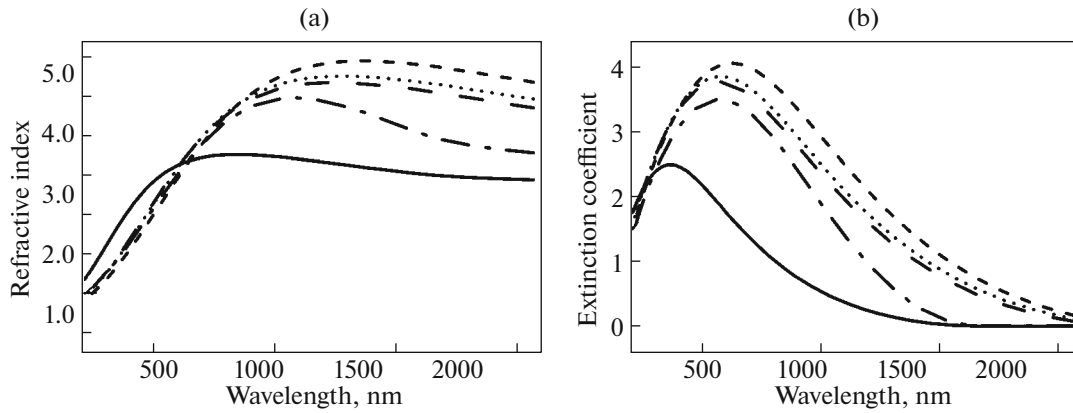


Fig. 7. Spectra of (a) the refractive index and (b) extinction coefficient of the $\text{Ge}_2\text{Sb}_2\text{Te}_5$ film samples annealed at different temperatures: (solid line) amorphous sample, (dash–dotted line) 180°C , (dashed line) 192°C , (dotted line) 200°C , and (broken line) 250°C .

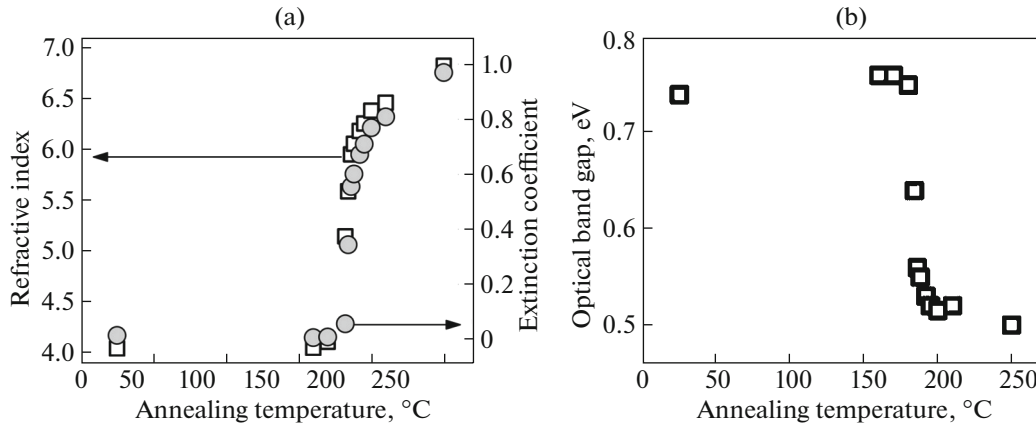


Fig. 8. Effect of the annealing temperature on (a) the refractive index, the extinction coefficient of $\text{Ge}_2\text{Sb}_2\text{Te}_5$ films at the wavelength 1550 nm , and (b) the optical band gap.

increase in the refractive index and extinction coefficient and a shift of their peaks to longer wavelengths. As the annealing temperature is elevated, these parameters increase as well, but not so sharply. It should be noted that, upon variations in the optical parameters, i.e., the refractive index and extinction coefficient, the spectra of amorphous and totally crystallized samples exhibit trends similar to those of the spectra shown in Fig. 1. At the same time, as the annealing temperature is elevated, we detected a decrease in the thickness h_2 of the $\text{Ge}_2\text{Sb}_2\text{Te}_5$ thin film from 106.5 to 98 nm (by 7.98%). This effect can be attributed to an increase in the density of the material by approximately 7.27% , when it transforms from the amorphous state (5.87 g/cm^3) to the cubic NaCl-structured crystalline state (6.33 g/cm^3) [27].

Figure 8 shows how the annealing temperature influences the refractive index and extinction coefficient

of $\text{Ge}_2\text{Sb}_2\text{Te}_5$ thin films at the telecommunication wavelength 1550 nm and their optical band gap.

From Fig. 8a it can be seen that heat treatment results in a noticeable increase in the refractive index and extinction coefficient. In this case, in the temperature range $170\text{--}200^\circ\text{C}$, we observe a sharp change in the optical parameters, which is due to crystallization of the $\text{Ge}_2\text{Sb}_2\text{Te}_5$ thin film. Upon heat treatment at temperatures higher than 200°C , these parameters increase further, which can be due in particular to an increase in the grain size in the polycrystalline structure. Figure 8b shows the results of calculation of the optical band gap. The temperature range of the phase transition correlates with the dependences shown in Fig. 8a. A decrease in E_g^{opt} from 0.71 to 0.47 eV is observed upon heating of the sample from room temperature to 250°C .

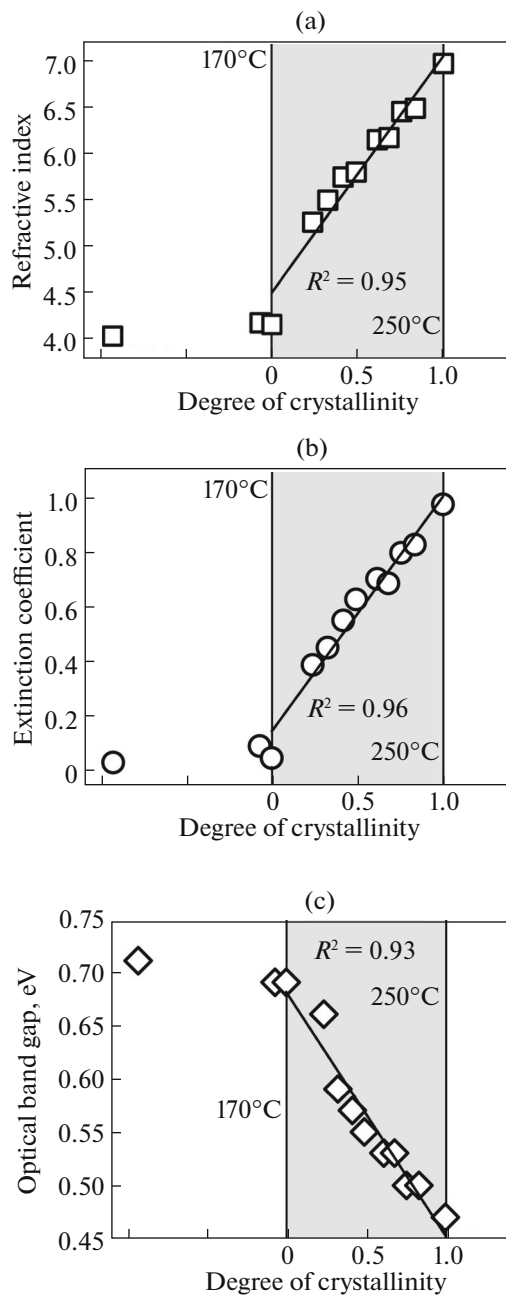


Fig. 9. Influence of the degree of crystallinity on (a) the refractive index, (b) the extinction coefficient of $\text{Ge}_2\text{Sb}_2\text{Te}_5$ films at the wavelength 1550 nm, and (c) the optical band gap.

We calculated the degree of crystallinity α [28] and assessed its effect on the optical parameters of $\text{Ge}_2\text{Sb}_2\text{Te}_5$ thin films:

$$\alpha = \frac{\ln\sigma - \ln\sigma_a}{\ln\sigma_c - \ln\sigma_a},$$

where σ is the conductivity of the thin film under study and σ_a and σ_c are the conductivities for the

totally amorphous and totally crystalline states, respectively.

For the totally amorphous state, we used the conductivity at the temperature corresponding to the onset of the phase transition; this temperature was determined from the temperature dependence of the resistivity by the first derivative method [29]. For the conductivity of the totally crystallized material, we chose the value obtained for the thin film at 250°C. As a result, the degree of crystallinity, i.e., the proportion of the crystallized material varies from zero (100% amorphous state) to unity (100% crystalline state). The dependences of the optical parameters on the degree of crystallinity are shown in Fig. 9.

Within the temperature range of crystallization of the $\text{Ge}_2\text{Sb}_2\text{Te}_5$ layer from 170°C to 250°C, the dependences of the refractive index and extinction coefficient on the degree of crystallinity are close to linear. This result correlates with a nearly linear dependence of the optical band gap on the degree of crystallinity. These results show that the degree of crystallinity of the $\text{Ge}_2\text{Sb}_2\text{Te}_5$ films influences their optical properties through variations in the optical band gap. In combination with the substantial change in the optical properties at the phase transition, such linear interrelation between the optical properties and the degree of crystallinity will make it possible to reliably record the intermediate states in phase-change memory cells.

CONCLUSIONS

Ellipsometry study of the optical properties of $\text{Ge}_2\text{Sb}_2\text{Te}_5$ thin films subjected to heat treatment at different temperatures gives results briefly summarized below.

The optical parameters and their dispersion determined in the study are influenced by the use of different layer and mathematical models. At the phase transition, the refractive index and extinction coefficient substantially increase. The optical band gap decreases from 0.71 to 0.47 eV upon transition from the amorphous state to the crystalline state. The dependences of the refractive index, extinction coefficient, and optical band gap on the degree of crystallinity are close to linear.

FUNDING

The study was supported by the Russian Foundation for Basic Research, project no. 20-07-01092, and the President of the Russian Federation, subject no. MK-6347.2018.3, agreement no. 075-02-2018-16; the study was carried out using equipment of the Regional Centre for Probe Microscopy of RSREU, and the Multiple-Access Centers “Diagnostics and Modification of Microstructures and Nanoobjects” and MIET core facilities center “MEMS and electronic components”, with support of the Russian Ministry of Education and Science.

REFERENCES

1. H.-Yu Cheng, F. Carta, W. C. Chien, et al., *J. Phys. D: Appl. Phys.* **52**, 473002 (2019).
2. Intel and Micron Produce Breakthrough Memory Technology. <https://newsroom.intel.com/news-releases/intel-and-micron-produce-breakthrough-memory-technology/#gs.vjlob>. Accessed February 10, 2020.
3. S. Kozyukhin, Yu. Vorobyov, P. Lazarenko, et al., *Non-Cryst. Solids* **480**, 51 (2018).
4. H. Zhang, L. Zhou, L. Lu, et al., in *Proceedings of the Conference on Lasers and Electro-Optics, Pacific Rim* (Opt. Soc. Am., 2017), p. s1972.
5. Z. Cheng, C. Rios, N. Youngblood, et al., *Adv. Mater.* **30**, 1802435 (2018).
6. J. Feldmann, N. Youngblood, X. Li, et al., *IEEE J. Sel. Top. Quantum Electron.* **26**, 1 (2019).
7. I. Chakraborty, G. Saha, A. Sengupta, et al., *Sci. Rep.* **8**, 1 (2018).
8. Y. Choi, M. Jung, and Y.-K. Leez, *Electrochem. Solid-State Lett.* **12**, 17 (2009).
9. X. Li, N. Youngblood, C. Rios, et al., *Optica* **6**, 1 (2019).
10. E. M. Vinod, K. Ramesh, and K. S. Sangunni, *Sci. Rep.* **5**, 8050 (2015).
11. G. Wang, X. Shen, Q. Nie, et al., *J. Phys. D: Appl. Phys.* **45**, 375302 (2012).
12. P. I. Lazarenko, Yu. V. Vorob'ev, M. E. Fedyanina, et al., *Perspekt. Mater.*, No. 10, 14 (2019).
13. Z. Xu, C. Chen, Z. Wang, et al., *RSC Adv.* **8**, 21040 (2018).
14. An. Redaelli, *Phase Change Memory. Device Physics, Reliability and Applications* (Springer, Cham, 2018).
15. K. Wang, C. Steimer, D. Wamwangi, et al., *Appl. Phys. A* **80**, 1611 (2005).
16. P. Nemeč, A. Moreac, V. Nazabal, et al., *J. Appl. Phys.* **106**, 103509 (2009).
17. M. Stegmaier, C. Rios, H. Bhaskaran, et al., *ACS Photon.* **3**, 828 (2016).
18. J.-W. Park, S. Ho Baek, T. D. Kang, et al., *Appl. Phys. Lett.* **93**, 021914 (2008).
19. M. Wuttig, H. Bhaskaran, and T. Taubner, *Nat. Photon.* **11**, 465 (2017).
20. J. Gonzalez-Hernez, E. F. Prokhorov, Yu. V. Vorobiev, et al., *J. Vac. Sci. Technol. A* **19**, 1623 (2001).
21. Kh. F. Nguen, S. A. Kozyukhin, and A. B. Pevtsov, *Semiconductors* **48**, 577 (2014).
22. G. E. Jellison and F. A. Modine, *Appl. Phys. Lett.* **69**, 371 (1996).
23. A. S. Ferlauto, G. M. Ferreira, J. M. Pearce, et al., *J. Appl. Phys.* **92**, 2424 (2002).
24. M. Di, Er. Bersch, Al. C. Diebold, et al., *J. Vac. Sci. Technol. A* **29**, 041001 (2011).
25. D. N. Seleznev, A. L. Sitnikov, A. V. Kozlov, et al., in *Proceedings of the RUPAC Conference, 2018*, p. 230.
26. R. Golovchak, Y. G. Choi, S. Kozyukhin, et al., *Appl. Surf. Sci.* **332**, 533 (2015).
27. K. Wang, D. Wamwangi, S. Ziegler, et al., *J. Appl. Phys.* **96**, 5557 (2004).
28. N. Mehta and A. Kumar, *J. Therm. Anal. Calorim.* **83**, 669 (2006).
29. I. W. Muchira, W. K. Njoroge, and P. M. Karimi, *J. Ovonic Res.* **11**, 131 (2015).

Translated by E. Smorgonskaya